

## Chemical synthesis and characterization of $Ce_xZr_{1-x}O_2$ powders by a modified sol-gel method

D.Hari Prasad<sup>a,b</sup>, Jong-Ho Lee<sup>a</sup>, Hae-Weon Lee<sup>a</sup>, Byung-Kook Kim<sup>a</sup> and Jong-Sung Park<sup>a,\*</sup>

<sup>a</sup> Center for Energy Materials Research, Korea Institute of Science and Technology, Seoul 136-791, Republic of Korea

<sup>b</sup> School of Engineering, University of Science and Technology, Daejeon 305-330, Republic of Korea

$Ce_xZr_{1-x}O_2$  ( $x = 1, 0.7, 0.4, 0.2, 0$ ) solid solution powders were successfully synthesized by a modified sol-gel method using a simple metal nitrate precursors as sources for cerium and zirconium which do not contain any hazardous and explosive precursor materials. X-ray diffraction (XRD) and Raman spectroscopy analyses revealed the formation of a solid solution depending on the ratio of the two oxides. In the modified sol-gel method, the composition range of the solid solution was wider than that from other methods. When the content of  $ZrO_2$  in the compound of  $Ce_xZr_{1-x}O_2$  was increased, the crystal structures were maintained as the cubic fluorite structures up to 60mol% of  $ZrO_2$  and the cubic phase was still predominant upto 80 mol% of  $ZrO_2$ . A decrease in the crystallite size and an increase in the BET surface area were observed along with an increase of the Zr content in  $Ce_xZr_{1-x}O_2$  solid solutions. The powder morphologies were also investigated by scanning electron microscopy (SEM) and transmission electron microscopy (TEM) analysis.

**Key words:** Ceria-zirconia, Solid solution, Raman Spectroscopy

### Introduction

Ceria-zirconia solid solutions have been recognized as key materials for various applications in catalysis, as ceramics, in fuel cell technology and as solid state electrolytes [1-5]. Zirconia addition to the cubic structure of ceria increases the oxygen storage capacity (OSC) while enhancing its thermal stability as compared to pure ceria alone, consequently these oxide solid solutions have also been studied extensively in the formulation of modern three-way catalysts (TWC) for automotive exhaust purification [1]. Replacement of cerium ions by cations of a different size modifies the ion mobility inside, and the changed lattice results in the formation of a defective fluorite structured solid solution. Such modifications in the defect structure of ceria are able to confer new properties to the material, such as better resistance to sintering at high temperature [6].

The effect of the modification of  $CeO_2$  with small amounts of oxides such as  $Al_2O_3$ ,  $SiO_2$ , and  $ZrO_2$  has also been investigated [7-10]. It has been reported that the addition of Zr can effectively increase the OSC. Ceria-zirconia solid solutions have been synthesized by various methods such as, precipitation [11], impregnation [9], precursor modification [12], sol-gel [13], surfactant- assistant [14], micro-emulsion [15], spray pyrolysis [16], sputtering [17], and chemical vapor deposition [18].

For  $Ce_xZr_{1-x}O_2$  solid solutions, the phase assessment is

less straight forward; cubic, tetragonal and monoclinic phases were obtained [19-21]. The selection of an appropriate precursor, the preparation method, composition, and textural properties, plays an important role in the success of these materials in the fields of catalysis and fuel cell technology. Trovarelli *et al.* [22] have demonstrated that the utilization of mechanical milling for the preparation of the catalysts based on  $CeO_2$  structurally modified with  $ZrO_2$  induces the formation of solid solutions. Hori *et al.* [23] have evidenced the formation of a  $ZrO_2-CeO_2$  solid solution when this was prepared by precipitation of the corresponding hydroxides and calcined at 500 °C. In contrast, two separate phases ( $CeO_2$  and  $ZrO_2$ ) were formed when the precipitation was performed by firing the corresponding acetate mixtures.

In the literature, for the synthesis of ceria-based solid solutions by the flame method and sol-gel routes, expensive precursors such as alkoxides have been used [24, 25]. Combusting mixtures of the redox compounds (urea) and oxidizing metal precursors (nitrates) pose explosive hazards leading to great difficulties in batch processes [26]. The goal of the present study was to prepare ceria-zirconia solid solutions ( $Ce_xZr_{1-x}O_2$  with  $0 \leq x \leq 1$ ) by a modified sol-gel method using simple, cost-effective nitrate sources and ammonia as the starting materials. The formation of a solid solution was confirmed by using various characterization techniques such as XRD and Raman spectroscopy. Further the powders were characterized by BET surface area measurements, SEM and TEM analyses and the results compared with the literature data. The influence of the composition on the structure and texture of the samples are discussed.

\*Corresponding author:  
Tel : 82-29586703  
Fax: 82-29585529  
E-mail: jongsung@kist.re.kr

## Experimental procedures

The  $Ce_xZr_{1-x}O_2$  ( $x = 1, 0.7, 0.4, 0.2, 0$ ) solid solution powders were prepared by a modified sol-gel method. Cerium (III) nitrate hexahydrate (Kanto chemicals) and Zirconyl (IV) nitrate hydrate (Acros organics; 99.5%Zr) were used as sources of Ce and Zr respectively. Ammonium hydroxide (Daejung chemicals) was used as the precipitating agent. The requisite quantity of each nitrate was dissolved in distilled water in separate beakers to make 0.1 M/l. Fig. 1 shows a schematic illustration of the synthesis method. Ammonium hydroxide was added drop wise at room temperature with continuous stirring to attain a pH of 9. The solution thus obtained was heated at 80 °C under continuous stirring to evaporate the excess water present and the sol has been transformed into a gel. The gel thus obtained was oven dried at 100 °C for 24 h. The dried materials were crushed into powders using a mortar and pestle and further calcined in air at 800 °C for 6 h, to get the final powder. The rate of heating as well as cooling was always maintained at 5 K·minute<sup>-1</sup>. The phase identification of  $Ce_xZr_{1-x}O_2$  powders was made using powder X-ray diffraction (PW 3830 X-ray generator). The Raman spectra were measured using a conventional back scattering geometry with a Raman spectrometer (T 64000, Jobin-Yvon, France) which consists of a triple polychromator and a CCD detector. The excitation source was an Ar ion laser ( $\lambda = 514.23$  nm) and the laser power was 10 mW at the sample point. The morphology of the powders was observed using a scanning electron microscope (NOVA SEM) and a transmission electron

microscope (TEM, Technai G2F20). The BET surface area was determined by N<sub>2</sub> adsorption at 77 K (a five point Brunauer-Emmett-Teller (BET) method using a Quantachrome Corporation Autosorb). Prior to the analysis, approximately 0.5 g of the powders was placed in a test tube and out gassed to eliminate volatile adsorbents at 200 °C for 3 h in flowing nitrogen. This removed the contaminants such as water vapor and adsorbed gases from the powders.

## Results and discussion

Fig. 2 shows the XRD patterns of  $Ce_xZr_{1-x}O_2$  ( $x = 1, 0.7, 0.4, 0.2, 0$ ) powders prepared by this method and then calcined at 800 °C for 6 h. From the figure, the XRD pattern of CeO<sub>2</sub> alone can be assigned to the cubic fluorite structure. The XRD pattern of ZrO<sub>2</sub> alone showed a mixture of monoclinic and tetragonal phases. A pattern similar to CeO<sub>2</sub> has been observed for the samples with  $x \geq 0.2$ , suggesting that ZrO<sub>2</sub> was incorporated into the CeO<sub>2</sub> lattice to form a solid solution while maintaining the fluorite structure. From the figure it can be observed that the diffraction peaks were shifted to higher degrees with a rise in the amount of ZrO<sub>2</sub> incorporated into CeO<sub>2</sub>. This observation indicates a shrinkage of the lattice due to the replacement of Ce<sup>+4</sup> with Zr<sup>+4</sup>, this coincides with the fact that the cation radius of Zr<sup>+4</sup> (0.86 Å) is less than that of Ce<sup>+4</sup> (1.09 Å). As compared with the XRD pattern of CeO<sub>2</sub> alone, the XRD peaks observed for  $Ce_xZr_{1-x}O_2$  solid solutions become broader indicating a distortion of the cubic phase of the fluorite structure to a tetragonal one due to the incorporation of ZrO<sub>2</sub> into CeO<sub>2</sub> [19]. The phase assignment for the mixed oxides is less straight forward. Cubic, tetragonal, and monoclinic phases have been reported for  $Ce_xZr_{1-x}O_2$  solid solutions [19-21]. Since mixed oxides obtained give broadened

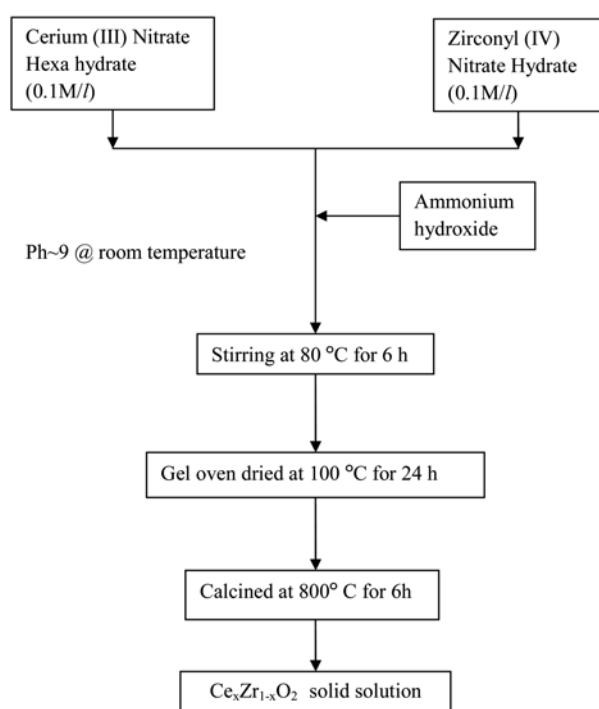


**Fig. 1.** Schematic illustration of the synthesis of  $Ce_xZr_{1-x}O_2$  solid solution powders by a modified sol-gel method

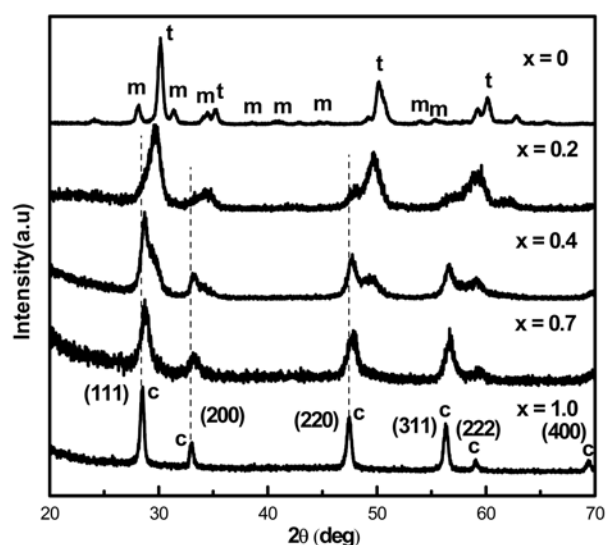


**Fig. 2.** XRD patterns of  $Ce_xZr_{1-x}O_2$  solid solution powders calcined at 800 °C for 6 h (t: tetragonal; m: monoclinic; c: cubic)

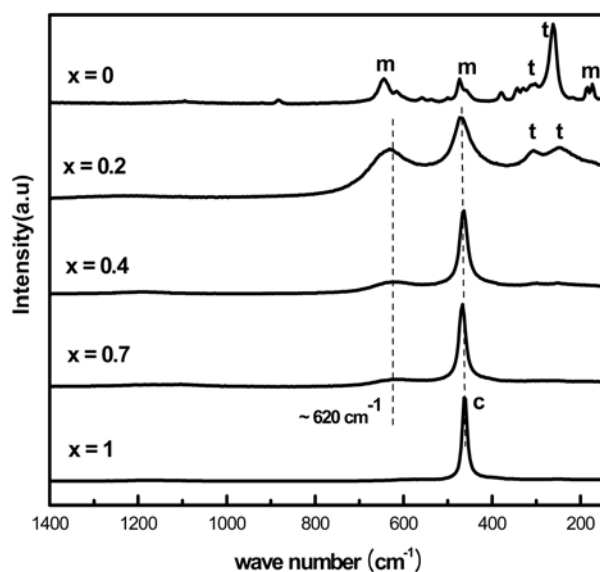
**Table 1.** Physical properties of the  $Ce_xZr_{1-x}O_2$  solid solution system

$Ce_xZr_{1-x}O_2$ solid solution	Crystallite size (nm)	BET Surface area ( $m^2/g$ )
$x = 0$	16.4	22.3
$x = 0.2$	7.3	47.2
$x = 0.4$	7.4	28.8
$x = 0.7$	11.4	18.3
$x = 1$	22.2	1.2

peaks in X-ray diffraction patterns, meaning that the symmetry of the solid solution phases or the co-presence of some amounts of a tetragonal phase in the mixed oxides cannot be determined accurately using XRD alone, Raman spectroscopy was thus employed to confirm their compositional phases and solid solution formation in these samples.

Table 1 summarizes the data for surface area and the crystallite size of the  $Ce_xZr_{1-x}O_2$  solid solutions prepared by this method. The surface area of  $CeO_2$  and  $ZrO_2$  are about 22.3 and 1.2  $m^2/g$ , respectively. The  $Ce_xZr_{1-x}O_2$  solid solutions showed higher surface areas of 47.2, 28.8 and 18.3  $m^2/g$  for  $x = 0.2, 0.4$  and  $0.7$ , respectively, than the  $CeO_2$  alone. It can be noticed that the BET surface area of  $Ce_xZr_{1-x}O_2$  solid solutions increase with an increase in the Zr content. This might be due to the substitution of a  $Zr^{+4}$  ion (0.86 Å), which has a smaller cationic radius, in the  $Ce^{+4}$  ion (1.09 Å) lattice location. A similar trend has also been observed by Xu and wang [27] and by Roh *et al.* [28] with an increase of the zirconium content. The surface area results suggest that the stabilization of the surface area of  $CeO_2$  is probably due to the inhibition of the sintering process by adding  $ZrO_2$  in the  $Ce_xZr_{1-x}O_2$  solid solutions.

In order to confirm the formation of solid solutions and the phases present in  $Ce_xZr_{1-x}O_2$  powders Raman spectroscopy analyses were preformed and the results are shown in Fig. 3. The Raman spectrum of  $CeO_2$  alone displayed a sharp peak at  $465\text{ cm}^{-1}$  and this corresponds to the cubic fluorite structure of  $CeO_2$  (Fm3m space group) with  $F_{2g}$  symmetry which can be regarded as a symmetric O-Ce-O stretching [29]. For the Raman spectrum of  $ZrO_2$  alone, the peaks displayed from 170 to  $200\text{ cm}^{-1}$  and at 265, 313, 460, 600 and  $645\text{ cm}^{-1}$  reveal the presence of monoclinic and tetragonal phases [30]. As for the  $Ce_xZr_{1-x}O_2$  powders, Raman spectroscopy proves to be a valuable tool in order to determine their symmetry. The Raman spectra for the  $Ce_xZr_{1-x}O_2$  samples containing  $x \geq 0.4$  did not vary significantly with that of  $CeO_2$  alone and showed only peak at  $465\text{ cm}^{-1}$  characteristic of the cubic fluorite-like structure. Conversely, when  $x = 0.2$  in the  $Ce_xZr_{1-x}O_2$  powders, the main peak in the Raman spectrum decreases in its intensity and additional peaks at 260 and  $309\text{ cm}^{-1}$  corresponding to tetragonal symmetry have been observed. This suggests the co-presence of a tetragonal and a cubic solid solution phase in  $Ce_{0.2}Zr_{0.8}O_2$ , as the band at  $460\text{ cm}^{-1}$  is observed together with the

**Fig. 3.** Raman spectra of  $Ce_xZr_{1-x}O_2$  solid solution powders calcined at  $800\text{ }^\circ\text{C}$  for 6h (t: tetragonal; m: monoclinic; c: cubic)

components typically of the tetragonal phase, although the cubic phase is still predominant. The broadening of the main intensity peak in  $Ce_xZr_{1-x}O_2$  powder when compared to  $CeO_2$  alone is related to the substitution of  $Ce^{+4}$  by  $Zr^{+4}$  cations. When compared to other synthesis methods such as precipitation [31] and template methods [32], where a predominant cubic fluorite structure cannot be obtained for the composition of  $Ce_{0.2}Zr_{0.8}O_2$ , our synthesis method showed the very promising result of a solid solution formation with this composition with a predominate cubic phase. This shows an ability of the formation of the cubic fluorite structure even with a larger amount of zirconium contents.

The  $Ce_xZr_{1-x}O_2$  solid solution powders exhibits a weak and broad peak feature at  $\sim 620\text{ cm}^{-1}$ . This peak could be attributed to a non-degenerate Raman inactive longitudinal optical (LO) mode of  $CeO_2$ . The appearance of this band is due to the presence of an oxygen concentration, which perturbs the local M-O bond chemistry leading to the relaxation of symmetry selection rules [33]. It should be mentioned here that this band is observed due to the nano-sized nature of  $Ce_xZr_{1-x}O_2$  oxides in which a larger amount of defect sites is expected. The presence of this band is expected to improve the catalytic performance of these materials [34]. It can be observed from the figure that as the zirconium content increased the intensity of this peak has also been increased indicating the nano-sized nature of  $Ce_{0.2}Zr_{0.8}O_2$  which is also observed from XRD and BET surface area results. The results from the Raman spectra are consistent with those from the XRD patterns of  $CeO_2$ ,  $ZrO_2$  and  $Ce_xZr_{1-x}O_2$  solid solutions.

Fig. 4 shows the SEM and TEM micrographs of the calcined  $CeO_2$ ,  $Ce_{0.4}Zr_{0.6}O_2$  and  $ZrO_2$  powders prepared by the modified sol-gel method. From the SEM images (Fig. 4(a-c)), it can be observed that the particles of

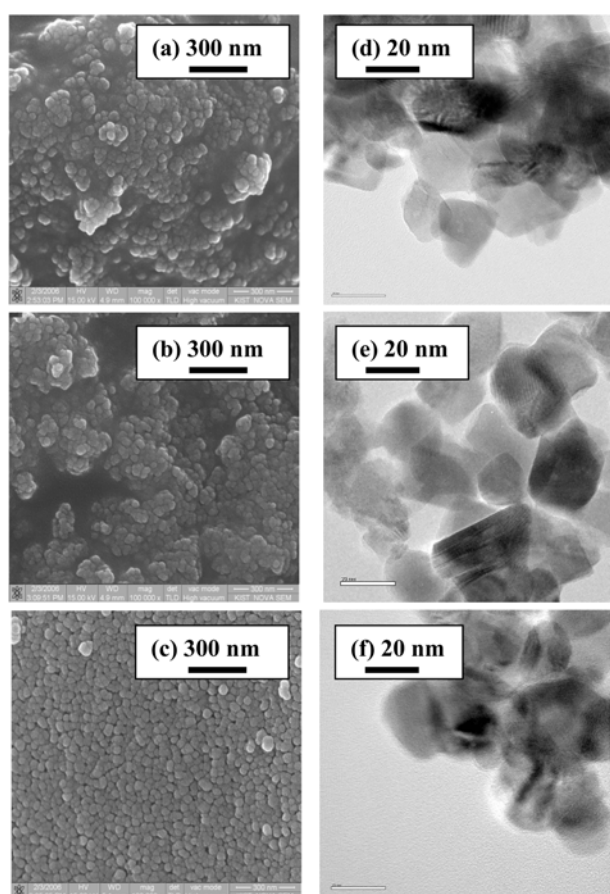


**Fig. 4.** SEM (a)  $CeO_2$  (b)  $Ce_{0.4}Zr_{0.6}O_2$ , (c)  $ZrO_2$  and TEM micrographs of (d)  $CeO_2$  (e)  $Ce_{0.4}Zr_{0.6}O_2$  (f)  $ZrO_2$  calcined at  $800\text{ }^\circ\text{C}$  for 6 h.

$CeO_2$  and  $Ce_{0.4}Zr_{0.6}O_2$  were agglomerated. TEM images (Fig. 4(d-f)) showed that the particle size ranged between 15-30 nm. The crystallite size obtained from XRD and the particle size observed from the TEM results further suggests that the particles were agglomerated.

## Conclusions

Nano-crystalline  $Ce_xZr_{1-x}O_2$  ( $x = 1, 0.7, 0.4, 0.2, 0$ ) solid solution powders were successfully prepared by a modified sol-gel method using cerium (III) nitrate hexahydrate and zirconyl (IV) nitrate hydrate as sources of Ce and Zr, respectively. For pure  $CeO_2$  and  $ZrO_2$  powders, a cubic fluorite structure and a mixture of monoclinic and tetragonal phases were identified by XRD and Raman spectroscopy analysis. Formation of  $Ce_xZr_{1-x}O_2$  solid solutions were also confirmed by XRD and Raman spectroscopy analysis. The Raman spectra for the  $Ce_xZr_{1-x}O_2$  samples containing  $x \geq 0.4$  did not vary significantly from that of the pure  $CeO_2$  and showed only a peak at  $465\text{ cm}^{-1}$  characteristic of the cubic fluorite-like structure. Conversely, for  $x = 0.2$ , an additional tetragonal phase was identified but the cubic phase was predominant. An increase in the BET surface area and a decrease in the crystallite size with an increase of the Zr content were observed for  $Ce_xZr_{1-x}O_2$  solid

solutions. SEM and TEM analysis showed that the particles were agglomerated when compared to  $CeO_2$  alone and the particle size ranged from 15-30 nm. With this method,  $Ce_xZr_{1-x}O_2$  solid solutions can be synthesized using simple starting precursors which do not contain any hazardous and explosive precursor materials.

## Acknowledgements

This work was supported by the Institutional Research Program of Korea Institute of Science and Technology.

## References

1. R.D. Monte, J. Kasper, *J. Mater. Chem.* 15 (2005) 633-648.
2. M.H.B. Bernal, S.D. De La Torre *J. Mater. Sci.* 37 (2002) 4947-4971.
3. B.C.H. Steele, *Nature* 400 (1999) 619-621.
4. J.R. Jurado, *J. Mater. Sci.* 36 (2001) 1133-1139.
5. D. Hari Prasad, H.-Y. Jung, H.-G. Jung, B.-K. Kim, H.-W. Lee and J.-H. Lee, *Mater. Lett.* 62 (2008) 587-590.
6. K. Kenevey, F. Valdivieso, M. Soustelle and M. Pijolat, *Appl. Catal. B* 29 (2001) 93-101.
7. M. Ozawa, M. Kimera, A. Isogai and J. Alloys Comp. 193 (1993) 73-75.
8. R.K. Usmen, G.W. Graham, W.L.H. Watkins and R.W. McCabe, *Catal. Lett.* 30 (1995) 53-63.
9. A. Bensalem, F.B. Verduraz, M. Delamar and G. Bugli, *Appl. Catal. A* 121 (1995) 81-93.
10. T. Masui, Y. Peng, K.-I. Machida and G.-Ya. Adachi, *Chem. Mater.* 10 (1998) 4005-4009.
11. N. Sergent, J.-F. Lamonnier and A. Aboukais, *Chem. Mater.* 12 (2000) 3830-3835.
12. G. -Ya. Adachi and N. Imanaka, *Chem. Rev.* 98 (1998) 1479-1514.
13. S.H. Overbury, D.R. Huntley, D.R. Mullins and G.N. Glevee, *Catal. Lett.* 51 (1998) 133-138.
14. D. Terrible, A. Trovarelli, J. Llorca, C. De Leitenburg and G. Dolcetti, *J. Catal.* 178 (1998) 299-308.
15. M.F. Garcia, M. Arias, I. Juez, C. Belvar and A.B. Hungria, *J. Catal.* 194 (2000) 385-392.
16. T.V. Mani, H.K. Varma, A.D. Damodaran and M.G.K. Warrier, *Ceram. Int.* 19 (1993) 125-128.
17. N. Izu, N. Murayama, W. Shin, M. Ichiro and K. Shuzo, *Jpn. J. Appl. Phys.* 43 (2004) 6920-6924.
18. W. Bai, K.L. Choy, N.H. J. Stelzer, J. Schooman, *Solid State Ionics* 116 (1999) 225-228.
19. P. Fornasiero, G. Balducci, R. Di Monte, J. Kasper, V. Sergo, G. Gubitosa, A. Ferrero, M. Graziani and J. Catal. 164 (1996) 173-183.
20. D.A. Ward, E.I. Ko, *Chem. Mater.* 5(1993) 956.
21. E. Tani, M. Yoshimura, *J. Am. Ceram. Soc.* 66(1983) 506.
22. A. Trovarelli, F. Zamar, J. Llorca, C. de Leitenburg, G. Dolcetti and J.T. Kiss, *J. Catal.* 169 (1997) 490.
23. C.E. Hori, H. Permana, K.Y. Simon, A. Brenner, K. More, K.M. Rahmoeller and D. Belton, *Appl. Catal. B Environ.* 16 (1998) 105.
24. R.M. Laina, C.R. Bickmore, K.F. Waldner and U.S. Patent (1995) 5614-596.
25. A. Gutsch, T. Henning, S. Katusic, M. Kramer, G. Michel and G.J. Varga, *European Patent* (2000) 1,142,830 A1.
26. S.T. Aruna and K.C. Patil, *Nanostruct. Mater.* 10 (1998) 955.
27. Shan Xu, X. Wang, *Fuel* 84 (2005) 563-567.

28. H.S. Roh, H.S. Potdar and Ki-Wonjun, *Catalysis Today* 93-95 (2004) 39-44.
29. J.R. McBride K.C. Hass, B.D. Poindexter and W.H. Weber, *J.Appl.Phys.* 76 (1994) 2435.
30. V.S. Escribano, E.F. Lopez, M. Panizza, C. Resini, J.M.G Amores and G Busca, *Solid State Sciences* 5(2003) 1369-1376.
31. K. Otsuka, Y. Wang and M. Nakamura, *Appl. Catal. A Gen.* 183 (1999) 317-324.
32. C. Liang, J. Qiu, Z. Li and C. Li, *Nanotech.* 15 (2004) 843-847.
33. B.M. Reddy, P. Bharali, P. Saikia, A. Khan, S. Loridant, M. Muhler and W. Grnert, *J. Phys. Chem. C*, 111 (2007) 1878-1881.
34. B.M. Reddy, P. Lakshmanan, S. Loridant, Y. Yamada, T. Kobayashi, L.-C. Carlos, C.R. Teresa and A. Fernndez, *J. Phys. Chem. B*, 110 (2006) 9140-9147.